Faraday Discussions

Accepted Manuscript

Faraday Discussions

Royal Society of Chemistry

ROYAL SOCIETY OF CHEMISTRY

www.rsc.org/faraday_d

Transport of Nanoparticulate Material in Self-Assembled Block Copolymer Micelle Solutions and Crystals

Vicki A. Cheng and Lynn M. Walker*

(Center for Complex Fluids Engineering)
Department of Chemical Engineering
Carnegie Mellon University, Pittsburgh PA

Abstract

Water soluble poly(ethylene oxide)-poly(propylene oxide)-poly(ethylene oxide) [PEO-PPO-PEO] triblock copolymers self-assemble into thermoreversible micellar crystals comprised of periodically spaced micelles. The micelles have PPO cores surrounded by hydrated PEO coronas and the dimensions of the unit cell of the organized micelles is on the order of several to tens of nanometers. Fluorescence recovery after photobleaching (FRAP) is used to quantify nanoparticle transport in these nanostructured polymer micelle systems. Diffusivity of bovine serum albumin (BSA, $D_h \sim 7nm$) is quantified across a wide range of polymer, or micelle, concentrations covering both the disordered fluid as well as the structured micellar crystal to understand the effects of nanoscale structure on particle transport. Measured particle diffusivity in these micellar systems is reduced by as much as four orders of magnitude when compared to diffusivity in free solution. Diffusivity in the disordered micellar fluid is best understood in terms of diffusion through a polymeric solution, while transport in the structured micellar phase is possibly due to hopping between interstitial sites. These results not only show that the nanoscale structures of the micelles have a measureable impact on particle diffusivity, but also demonstrate the ability to tune nanoscale transport in self-assembled materials.

*corresponding author: *lwalker@andrew.cmu.edu*

Introduction

Block copolymers exhibit complex phase behavior, particularly when dispersed in a solvent that selectively solubilizes specific polymer blocks. At low polymer concentration, block copolymers in selective solvents form micelles, with aggregation numbers in the tens to hundreds and dimensions of nanometers.   As polymer concentration increases, these micelles self-assemble into packed nanocrystalline structures with geometries including cubic arrangements of spherical micelles and hexagonal ordering of cylindrical micelles.[1-5] These micellar crystals have short range and long range crystalline order and mechanical behavior that is best described as a soft solid.

Poly(ethylene oxide)-poly(propylene oxide)-poly(ethylene oxide) block copolymers (PEO_n-PPO_m-PEO_n), commercially known under the trade name Pluronic®, or Polyoxamer®, are a class of water-soluble block copolymers that undergo a reversible temperature-induced transition from a disordered micellar fluid to a crystalline nanostructured system.[5-8]   While the PEO and PPO blocks are both water soluble at temperatures below about 10°C, the block copolymers micellize at higher temperatures, with the PPO dehydrating first and self-assembling to form the micellar core. At sufficiently high temperatures and concentrations, the block copolymer micelles will pack into crystalline structures. This self-assembling behavior has been characterized in phase diagrams for several types of Pluronic systems using a combination of small-angle scattering techniques; these same techniques provide details about the block copolymer packing structure, micelle size and shape.[7-14]

There is recent interest in generating hydrophilic nanocomposites based on interspersing nanoparticulate material in these nanostructured block copolymer micelles.[15-20] Sequestering hydrophilic nanoparticulate material to the continuous phase of these packed block copolymer systems has the potential to control spatial arrangement of the nanoparticulate material using the self-assembled structure of the block copolymer micellar solution. This technique has been demonstrated in several different architectures of Pluronic®; F127 (PEO_{106}-PPO_{70}-PEO_{106}), F87 (PEO_{75}-PPO_{46}-PEO_{75}) and P123 (PEO_{20}-PPO_{70}-PEO_{20}) for a variety of nanoparticulate materials with hydrodynamic diameters ranging from 4-7 nm, including silica, lysozyme, and bovine serum albumin (BSA).[15-19, 21-23] This structure has been verified by contrast matching small-angle neutron scattering (SANS).[15, 16, 18] In developing this templating process, the nanoparticle systems have been selected such that they are comparable in size to the interstitial domains of the structured block copolymer.

Previous studies on these nanoparticle-block copolymer composites have characterized the static structure and mechanics of these systems, but little is known about the transport behavior of nanoparticles within the ordered block copolymer. The structure and composition of these composites presents several

possibilities for the dynamic behavior of the nanoparticles. Because the nanoparticle dimensions are closely matched to that of the block copolymer interstitial spacing, it is possible that the nanoparticles are trapped within the structured matrix formed by the block copolymer, and no significant particle transport occurs. However, these block copolymer composites are also 'soft' systems largely comprised of water, so nanoparticles also diffuse through the solvent-filled free volume available in the block copolymer. Furthermore, these composites form an intercalated crystal structure, and so it is plausible for particle transport to resemble diffusive behavior in solid crystalline materials. Clearly, several possible transport mechanisms exist in these nanostructured block copolymers, and it is critical to understand the dynamic behavior of nanoparticles in these systems, especially when considering their potential applications as nanocomposites,[24, 25] systems for storing ordered nanoparticle arrays,[17, 19] protein protection,[26] as media for DNA separation,[27, 28] or as nanostructured templates for mineralization.

Here, we quantify nanoparticle diffusion through the micellar block copolymer systems. Considerable work has been performed to understand and model particle diffusion in polymer solutions and melts.[3, 29-34] Studies on diffusion through polymer gels and hydrogels have typically been performed on materials whose structures have no long-range order, and so the nanoscale structure of these block copolymers provide a unique medium for studying particle transport, especially when the interstitial voids are on similar lengthscales as the particles. Fluorescence recovery after photobleaching (FRAP) is used to determine the diffusive properties of small molecules and macromolecules through biological environments and polymeric gels,[35-37] and is suitable for studying nanoparticle transport through these self-assembled block copolymers. For this study, fluorescently-tagged BSA, a globular protein, is used as a model monodisperse tracer particle to complement the prior structural studies done on the nanocomposite system. Protein (probe) diffusivity is studied across a range of polymer concentrations covering both the disordered fluid phase as well as the structured micellar phase to understand how micellar ordering affects particle transport. The effects of protein loading, shear alignment, particle type, and block copolymer composition are also examined in this study.

Materials and Methods

Materials

Pluronic® block copolymers F127 (PEO_{106}-PPO_{70}-PEO_{106}), F87 (PEO_{75}-PPO_{46}-PEO_{75}), and P123 (PEO_{20}-PPO_{70}-PEO_{20}) (BASF; Mount Olive, NJ) are used as received. These are commercial materials with both molecular weight and structural polydispersity, but these are studied extensively in the literature and applied broadly, so the materials are used as received here. Properties of the three block copolymers used are reported in Table 1; the reported overall molecular weights, degree of polymerization of the blocks

and ratio of number of PEO to PPO units are provided. The CMC is reported from the literature. 5-hexadecanoylamino-fluorescein (HDFL) is purchased from Sigma Aldrich (St. Louis, MO) and used as received. Fluorescein isothiocyanate (FITC) is used as received for labeling the protein bovine serum albumin (BSA) (Sigma Aldrich; St. Louis, MO).

<< Table 1 >>

Protein Labeling

Bovine serum albumin is fluorescently labeled with fluorescein isothiocyanate (FITC) at a 1:1 fluorescence to protein (F/P) molar ratio using 0.1 M sodium carbonate-bicarbonate buffer (pH = 9.0), following standard protocols described elsewhere.[38, 39] The labeled protein is separated from unreacted FITC using a Sephadex G-25M Column (Sigma Aldrich; St. Louis, MO), followed by dialysis. The concentrations of BSA and FITC are determined spectrophotometrically using extinction coefficients previously determined in buffer: $_{FITC}^{495}\varepsilon = 70,000 M^{-1}cm^{-1}$,[40] $_{FITC}^{280}\varepsilon = 10,950 M^{-1}cm^{-1}$,[41] or measured $_{BSA}^{280}\varepsilon = 34,512 \pm 820 M^{-1}cm^{-1}$. The addition of the FITC tag (389 g/mol) to BSA (69324 g/mol) at this low level of tagging does not significantly alter the hydrodynamic size of the BSA probe and is not expected to change the interaction of BSA with the block copolymer matrix.

Block Copolymer-Protein Composite Preparation

The FITC-BSA is combined with unlabeled BSA to reduce the average F/P ratio, maintaining the total FITC concentration at 47 μM. This FITC concentration has been verified to be within the linear region of fluorescence intensity as a function of fluorophore concentration. The BSA is then incorporated into three Pluronic® block copolymer systems (F127, F87, and P123), following procedures outlined previously.[15, 16, 23] All dispersions were prepared in 0.1M sodium carbonate-sodium bicarbonate buffer (pH=9.0) to maximize the fluorescence of the FITC. The BSA concentration in the block copolymer-protein composites range from 0.25 to 5.4 wt%, while the block copolymer concentration ranges from 7 to 43 wt% of the total composition.

Rheological Characterization

Viscosity measurements are performed for the fluid solutions using a stress-controlled rheometer (Bohlin Gemini, Malvern Instruments; West Borough, MA) with a Couette geometry (cup and bob, O_D=27.5mm, I_D=25mm, gap=1.25mm). The temperature is controlled with a Peltier unit, and measurements are made at 25°C. For the micellar crystals, measurements are made with a parallel plate geometry (D=25mm) and a gap of 800 μm. The concentration at which the block copolymer first resembles a solid, C_{gl}, is defined here as the concentration at which G' first exceeds G'' at 25°C and is identified by performing

temperature sweeps (1°C/minute, 1 rad/s) on block copolymer samples and given in Table 1. Measurements were performed on samples in increments of 1wt% to find the critical concentration. This is a somewhat arbitrary definition; however, it is used consistently for all block copolymer samples to provide a convenient comparison. The block copolymer systems are allowed to cool at 5°C for at least 5 minutes before proceeding with experiments. A thin layer of mineral oil is placed around the sample geometry to prevent evaporation during the experiment. First, the linear viscoelastic region is determined by performing by increasing the stress amplitude at fixed frequency (1 rad/s) and identifying the region where the moduli are invariant to stress amplitude. The magnitude of the complex modulus ($|G^*|$, or for simplicity, G^*) is then measured in the linear viscoelastic region; for the systems here, at an applied stress of 50 Pa at a frequency of 1 rad/s.

Fluorescence Recovery After Photobleaching (FRAP)

Block copolymer-protein samples are loaded into rectangular capillaries (0.4 x 4 mm cross sectional area, Vitrocom; Mountain Lakes, NJ), and the ends are sealed with wax. The capillaries are mounted on a microscope slide and imaged on a fluorescence microscope (Nikon Eclipe Ti-U; Melville, NY) at the 10x objective (NA=0.3) using a mercury arc lamp (XCite 120 Q, Lumen Dynamics; Ontario CA). An ND4 filter is used to reduce exposure of the sample to the light source. An image is captured prior to the bleaching, and the sample is then bleached with a 488 nm laser (Sapphire™, Coherent Inc; Santa Clara, CA) for 5 seconds. Subsequent images are taken using the mercury lamp for illumination; the shutter remains closed in between image acquisition to reduce the effects of sample bleaching from the imaging process.

Images are normalized based on a double normalization procedure.[42] Briefly, the intensity of the bleached spot at each time point $I_s(t)$ is first normalized with respect to the pre-bleached image, $I_{s,i}$. Then, the intensity is corrected for bleaching during the imaging process using the ratio of the pre-bleach intensity of an unbleached portion of the sample, $I_{ub,i}$ to its intensity a particular time point, $I_{ub}(t)$, as a correction factor, yielding a final normalized intensity of $I_N(t) = \dfrac{I_s(t)}{I_{s,i}} \dfrac{I_{ub,i}}{I_{ub}(t)}$. The normalized recovery curves are obtained by plotting the normalized intensity within the central region of the bleached spot over time. The subsequent recovery curves $I_N(t)$ are then fitted to the recovery function of the form

$$I_N(t) = f_m [\sum_{n=0}^{\infty} \frac{-K^n}{n!} [1 + n(1 + 2t/\tau)]^{-1}] + (1 - f_m) \frac{I_N(0+)}{I_{N,i}}$$, where f_m is the mobile fraction of the probe,

K is a bleaching parameter describing the bleach depth, τ is the time constant for fluorescence recovery, and $I_N(0+)$ is the sample intensity immediately following bleaching.[43] Fits to the recovery function

indicate that the probe species is at essentially full mobility in all samples, with mobile fractions f_m above

0.9 for all systems studied. Diffusion coefficients are determined from the relaxation time using $D = \dfrac{w^2}{4\tau}$

where w is the initial radius of the bleached spot and the typical spot size is (48 ± 3) µm. Average values

of D are found by taking measurements at a minimum of three different positions in the each sample.

To verify that the long range alignment of the samples does not significantly impact the diffusivity, FRAP experiments on shear aligned samples are performed on a fluorescence microscope equipped with an XY microscope stage controller (Applied Scientific Instrumentation; Eugene, OR). A block copolymer sample is loaded onto a glass microscope slide and placed in the slide holder. A second glass slide is positioned over the first slide such that the gap between the two slides is 0.5 mm, and is held stationary for the duration of the experiment. An initial FRAP experiment is performed on the unaligned soft solid sample. The XY stage is then programmed to oscillate in a simple linear manner at 1 Hz and 500% strain for 10 minutes. This is shown to be a large enough deformation to align the crystal for these materials.[2, 17, 22] On cessation of shear, FRAP experiments are performed on the sample. No asymmetry in the recovery is observed. The fluorescence recovery behavior for both sheared and unsheared F127 gels (25 wt% and 30 wt%) containing 1 wt% BSA was quantified. Results indicate that the recovery of sheared samples is similar to that of unsheared samples, suggesting that adjusting the alignment of the micellar crystals does not affect the overall transport behavior. This also suggests that nanoparticles are not sequestered at the grain boundaries of the polycrystalline material as has been seen in other studies.[20]

Results

Figure 1 shows the mechanical behavior of Pluronic[®] F127, F87, and P123 both below and above C_{gl}, values are given in Table 1. Below C_{gl}, the rheology is characterized by the zero shear viscosity while above C_{gl}, the rheology is characterized by the magnitude of the complex modulus G*(ω). Again, this transition point is defined as the point that the in and out of phase components of the moduli are equivalent at 25°C and 1 rad/s. The samples defined as "fluid" flow in reasonable timescales while those defined as "micellar crystal" do not. In many publications, this is referred to as a gel and, in other cases and more correctly, a glassy system.[44] Here, we avoid that terminology as the rheology of these soft solids, or micellar crystals, is much more complicated than that of a traditional polymer gel and lacks structural connectivity.[45] The disordered micellar fluids show an exponential increase in viscosity as block copolymer concentration increases, which is consistent with results seen by others and attributed to the increasing number of micelles present in the system which are interacting hydrodynamically.[46] Above C_{gl}, the block copolymer micelles arrange into packed configurations and have modulii on the order of

100 kPa, with G*(ω) exhibiting moderate increases with increasing concentration. We would expect the modulus to scale with ~kT/R^3 and the moduli follow the correct dependence with micelle size, but the range of R sampled is not large enough to verify this scaling. The mechanical behavior is tunable by changes in block copolymer concentration, and the transition between fluid and solid behavior in the bulk can be monitored rheologically.

<< Figure 1 >>

Figure 2 shows the resulting FRAP measurements of two types of probes in ordered block copolymer systems. Hydrophilic BSA tagged with fluorescein isothiocyanate (FITC-BSA), and a hydrophobic dye, 5-hexadecanoylamino-fluorescein (HDFL), a C_{16} alkane derivative of fluorescein.   The data show the normalized intensity as a function of time for each of the two probes in 25 wt% F127 (C/C_{gl} = 1.4). In this system, FITC-BSA exhibits fluorescence recovery, a measure of the probe diffusing over lengthscales of the spot in the timescales of the experiment. The fluorescence recovery of FITC-BSA in the sample occurs on the order of hours, and a diffusion coefficient of 0.32 ± 0.01 μm^2/s is extracted from this data. The diffusivity of free FITC is much faster comparable to that expected for diffusion of solvent molecules and too rapid for analysis using our FRAP experiment.

<< Figure 2 >>

In contrast, the hydrophobic dye shows little recovered intensity over even longer time scales. Because of the hydrophobic nature of HDFL, the dye resides closer to the hydrophobic interior of the micelle. That so little fluorescence recovery is observed with the hydrophobic dye indicates that movement of the ordered micelles is much slower compared to that of FITC-BSA. This result suggests that the packed structures in the micellar crystal phase restrict the movement of the micelles and is consistent with other measurements.[47] The hydrophobic dye is also tested in the disordered micellar fluid phase (7 wt% F127), and fluorescence recovery is observed, with a diffusion coefficient of 3.2 ± 0.1 μm^2/s, consistent with diffusion of an object of the size of a micelle in water.

The diffusion coefficient of FITC-BSA is measured in three different block copolymer systems with concentration ranges spanning across the fluid and micellar crystal phases. The protein concentration (1 wt%, or 10 mg/mL, BSA) is the same for all experiments and kept low to avoid protein-protein interactions. Figure 3 shows the normalized FITC-BSA diffusivity as a function of block copolymer concentration. Protein diffusivity in the block copolymer solution has been normalized to the protein diffusivity in free solution, D_o, which is 55.1 ± 0.5 μm^2/s. The filled symbols correspond to fluid samples while the open symbols to soft solids. Results indicate that the protein diffusivity decreases with the

addition of block copolymer. Even at the lowest block copolymer concentrations micelles are present but disordered, and the BSA diffusivity in this case is already one order of magnitude slower than for BSA in free solution. In all three systems, the normalized diffusivity decreases smoothly as the block copolymer concentration increases in the fluid phase. As concentration increases above C_{gl}, protein diffusivity decreases by at least two orders of magnitude. For the F127 and F87 systems, the dependence of diffusivity on concentration is smooth through the transition from a fluid to a soft solid. For the P123 samples, the decrease in protein diffusivity when the polymer is above C_{gl} is more significant showing a significant drop at C_{gl} and then an even steeper drop as concentration increases. Nanoparticles of size similar to BSA are expected to be most significantly hindered in mobility in the P123 at $C/C_{gl} > 1.2$. Note from Table 1 that P123 has the shortest PEO chains relative to PPO, suggesting micelles with large cores and thinner corona are best for hindering particle mobility.

<< Figure 3 >>

To demonstrate the impact of block copolymer structure on the diffusion of BSA, Figure 4 shows the same data as Figure 3, with the concentration is scaled with the concentration at which the sample transitions to a soft solid, C_{gl}. The diffusion coefficient is again scaled with the free diffusivity of BSA in water, so it is the same for all solutions. The solid symbols are for block copolymer solutions that are fluid while the open symbols are soft solids; hence the sharp division at $C/C_{gl} = 1$. In this figure, two of the block copolymers, F127 and P123 show similar behavior in the fluid state but then separate quickly in the soft solid state as the diffusivity of P123 drops rapidly with increasing concentration. The F87 sample shows slower diffusion than the other two except for the highest concentrations of P123. It is also clear that none of these samples follow a simple power law dependence with overall block copolymer concentration.

<< Figure 4 >>

Significant increases in particle loading have been shown to change the composition, rheology, and structure of the composite systems.[15, 21] Figure 5 demonstrates the impact of protein diffusivity on various F127 micellar crystals as the BSA loading is increased. Analysis of the micelle crystal structure by SANS[21] have shown that the block copolymer micelle structure is not affected in studies where the BSA loading has been kept at 1 wt%, which is a concentration where there are fewer than one BSA per micelle. Mechanical characterization of the block copolymer nanocomposite has also shown as much as a 40 kPa decrease in complex modulus with the addition of nanoparticles at higher loadings, indicating a significant weakening of soft solid.[15, 16, 18] Despite the significant structural and mechanical changes in

the block copolymer nanocomposites at higher nanoparticle concentrations, the BSA diffusivity exhibits essentially no change with increased particle loading.

<< Figure 5 >>

BSA is a globular protein and it is often treated as a spherical probe. This has been successful in studying transport of BSA in other polymer matrices. Stokes-Einstein-Sutherland diffusion of a sphere in a solvent provides an established relationship between probe size, solvent viscosity and diffusivity. Assuming that the medium is homogeneous, the product of the particle diffusivity and system viscosity $D\eta$ is related to the inverse of the hydrodynamic size of the probe R in the medium and a group of constants as shown in Equation 1, where k is the Boltzmann constant and T is the temperature,

$$D\eta = \frac{kT}{6\pi R} \ .\tag{1}$$

When normalized with D_o, the particle diffusivity through the pure solvent, and η_o, the viscosity of the pure solvent, the quantity $D\eta/D_o\eta_o$ should be a constant of value unity for a probe experiencing simple transport through the solvent. The value of $D\eta/D_o\eta_o$ is used to evaluate whether a system conforms to this behavior, and can also provide some measure of the local behavior of the solution.[32] The quantity $D\eta/D_o\eta_o$ for F87, F127, and P123 is plotted against block copolymer concentration in Figure 6 using measured values for the viscosities of the solutions (see Figure 1). Particle diffusivities deviate from simple behavior for nearly all concentrations, indicating that protein transport is influenced by local solution properties other than the macroscopic viscosity, but this is not unexpected given the relatively high concentration of micelles present. Similar analysis performed with BSA dispersed in aqueous solutions of 6000 g/mol PEO showed reasonable agreement with Stokes-Einstein-Sutherland for concentrations below 10wt% PEO.

<< Figure 6 >>

For cross-linked and entangled polymer systems, the crosslink density is proportional to the elastic modulus of the material,[48] and impacts particle transport, in that an increase in crosslink density is directly related to a measureable reduction in particle diffusivity.[49, 50] In this system, there are no entanglements and the modulus arises from the glassy-like behavior of the packed micelles. Although these block copolymers form micellar crystals by physical rather than chemical association, they still possess a measurable modulus which may be related to transport of particles. In Figure 7, the reduced diffusivity of BSA is shown versus the complex modulus G* for a series of micellar crystal block copolymer

compositions. Here, we report the complex modulus, G*, noting that for these soft solids, the phase angle is close to zero and the complex modulus is dominated by the elastic modulus, G'. Protein diffusivity decreases with increasing values of the modulus for each block copolymer system. However, results indicate that macroscopic properties such as G* are not the sole predictor for nanoparticle transport, as the F87 systems exhibit the highest values of G* but intermediate diffusivity values.

<< Figure 7 >>

It is interesting to note that two systems (F127 and P123) seem to follow a behavior of a similar decrease in diffusivity with increase in modulus. While it would be too much to argue a universal behavior from the overlap of the limits, these are the two systems that exhibit an FCC unit cell.   The F87 system forms a BCC unit cell and has significantly higher modulus for similar transport of BSA through the soft solid.

Discussion

Diffusivity of nanoparticulate material in these self-assembled block copolymer systems is complicated by the different lengthscales involved. In the fluid phase, the block copolymers are in a combination of unimers and micelles on the order of nanometers to tens of nanometers and are comparable to the size of the BSA probe particle (D_h~7nm). As the block copolymer micelles pack into ordered crystalline structures, similarities between the lengthscales of the polymer and particle remain. The dimensions of the block copolymer micelles and interstitial regions can be determined from SANS measurements on the ordered block copolymer; for this study, the interstitial regions in between packed micelles range from 1.8 to 4.5 nm, which corresponds closely to the hydrodynamic radius of BSA.

Diffusion in the micellar fluid

The lack of agreement with Stokes-Einstein-Sutherland using the solvent or bulk viscosity indicates that, rather than a homogeneous bulk, the probes are likely sampling the PEO coronas of the micelles, better modeled as a polymer solution.[30-32]   BSA diffusion probes the nanostructure of the block copolymer solution. Since this work is performed on isothermal samples, the block copolymers persist as micelles in solution at all concentrations.   The micelles partition the PPO into cores so diffusion is through solvent and the PEO coronas. As concentration increases and the system forms a soft solid, the BSA will sense a solution that is more and more reminiscent of a PEO solution in water.   The PEO blocks in these materials (see Table 1) are short, below 5000 g/mol. If free in solution, the radius of gyration of these PEO chains would be less than the radius of the probe (R_o = 3.5nm). To compare the measured diffusion coefficients to those expected in PEO solutions, the volume of the cores is calculated using the bulk

density of PPO and assuming that the cores are fully dehydrated. Assuming that the BSA does not penetrate these cores, the remaining volume contains the PEO chains.   These are structured into micelle coronas, but for an initial comparison, the effective volume fraction of PEO, ϕ_{PEO}, is calculated as the concentration of PEO chains (two per block copolymer chain) in the solvent omitted from the PPO cores. The PPO cores make up less than 10% of the volume for most of the solutions studied. The radius of gyration of PEO chains in water has been shown to be $R_g = 0.02M_w^{0.58}$, giving a R_g of less than 2-3 nm.[51]

The value of ϕ^*, or the overlap concentration, is calculated using $\phi^* = 3M_w / (4\pi\rho N_A R_g^3)$ and found to correspond to concentrations in the fluid state for the F127 and F87, but is above the studied concentrations for all of the P123 solutions. This is due to the shorter PEO blocks of the P123 system. Above ϕ^*, the relevant lengthscale is the correlation length, $\xi \approx R_g(\phi / \phi^*)^{-0.76}$, which is concentration dependent.   For the three block copolymers studied here, $\xi < R_o$, for most of the solutions.   For F127 and P123, only the lowest concentrations have correlation lengths larger than the probe size, but those samples have effective PEO concentrations below ϕ^*. For F87, all of the concentrations have correlation lengths shorter than the probe size.

Figure 8 shows the diffusivity scaled for comparison to the stretched exponential dependence reported for PEG solutions. Here, the scaled diffusivity is plotted with concentration expressed in terms of relevant lengthscales, the R_g of the PEO block and the correlation length which is inversely proportional to the effective PEO volume fraction. Based on observed scaling in the literature for PEG solutions, we expect the diffusivity to follow a stretched exponential, $D_0 / D = \exp(\beta(R_g / \xi)^\delta)$.[33]   This functional form is simply convenient for comparison. Again, filled symbols are for samples that are macroscopic fluids and the open symbols are for soft solids.   Two of the samples, F127 and F87, collapse in this representation. Since these have similar molecular weights of the PEO blocks, this might not be surprising, but the collapse is extremely good with a large region of overlap and through C_{gl}.   The P123 samples are significantly different with much slower diffusivity even in the fluid state.

<< Figure 8 >>

The dotted line shows the expected behavior of PEG solutions, with β = 1.63 and δ = 0.89 which underestimates the relationship;[33] this is not unexpected as the block copolymer micelle environment is diffusion through packed coronas rather than free PEO chains.   The data for F127 and F87 does agree with a stretched exponential with $\beta \sim 3$ and $\delta \sim 1.1$ but this imparts no physical insight into the diffusion mechanism although it might prove a useful tool to predict transport behavior. The collapse of the F127

11

and F87 samples suggests that probe diffusion in these materials is similar to diffusion through a semidilute polymer solution, with hindrances due to the structure of the corona or probe-polymer interactions.

A recent approach to modeling diffusion of non-interacting (i.e., non-sticky) probes in unentangled and entangled polymer solutions and melts is also considered.[29, 52] A scaling analysis has been presented in which particle diffusivity is shown to be affected by the size of the particle, $d = 2R_o$, relative to the polymer correlation length, ξ.[29] For a polymer in a good solvent, the volume fraction of polymer at which ξ is on the same order of the particle size scales as

$$\phi_{d,\xi} \cong (d/b)^{-1.32} \ , \tag{3}$$

where d is particle diameter, and b is the Kuhn length of the monomer. Below this concentration, diffusivity is expected to follow Stokes-Einstein-Sutherland behavior with respect to the solvent viscosity, while above this concentration diffusivity is expected to have a power law dependence on the polymer concentration,

$$D(\cdot)/D_0 = \alpha \ (\phi/\cdot_{d,\xi})^{-1.52} \ , \tag{4}$$

where α is a scaling factor determined from fitting of the data, D_0 is diffusivity of the probe in pure solvent, ϕ is polymer concentration, and $\phi_{d,\xi}$ is the concentration at which ξ is the same size as the probe particle diameter.

For the block copolymer micelles, the PPO blocks are sequestered in the micelle cores, while the PEO coronas are exposed to water. The systems here are modeled as PEO solutions, in which polymer concentration, c, is determined by calculating an effective PEO concentration which excludes the volume occupied by fully dehydrated PPO cores. Water is a good solvent for PEO and all of the polymer concentrations in this study are above the "crossover" concentration $\phi_{d,\xi}$ ($\phi_{d,\xi}$ ~7% for a BSA and PEO probe-polymer system),[53, 54] so the diffusivity data is examined with Equation 4. The fitting parameter α is obtained for each block copolymer system by vertically shifting the lowest concentration (For F127 and F87, α ~ 0.13 while the value is slightly lower for P123, α ~ 0.1). The reduced diffusivity is plotted against normalized concentration, $\phi/\phi_{d,\xi}$ in Figure 9, and the systems in the fluid phase are differentiated from the micelle crystal phase with filled and unfilled symbols, respectively. The power law dependence predicted by the scaling relationship is denoted with the dashed line, and the data for the lower concentrations in each polymer system falls onto this curve. The data deviates from this scaling at higher concentrations, suggesting a change in the diffusion mechanism as the local environment becomes

12

increasingly crowded with micelles. In all cases, the scaling appears to hold for concentrations below about $\phi/\phi_{d,\xi} \sim 2$.

<< Figure 9>>

Diffusion in the ordered block copolymers

As the block copolymer concentration increases, the system reaches a point when the micelles pack into ordered configurations. Neutron scattering measurements on these ordered materials have produced structural information on the specific packing configurations, as well as relevant length scales, such as the crystal lattice parameters and hard sphere dimensions.[18, 19, 21, 23] Table 2 lists these parameters for some specific block copolymer compositions; for the diffusion studies, the block copolymer soft solid are cubic (FCC or BCC), and the crystal type remained consistent for each block copolymer system.

Figure 10 shows a schematic of the nanoscale structure of three block copolymer systems used in this work.   Dimensions for a specific concentration and temperature are determined using small angle scattering (SAXS and SANS) and assuming that the PPO core is fully dehydrated. Important dimensions of the micellar crystal are the unit cell size, a, measured directly from scattering, the center-to-center distance of the micelles, D_{cc}, determined from the unit cell size and knowledge of the crystal structure, the size of the PPO core, R_{core}, determined from the copolymer molecular properties and assuming that the core is fully dehydrated.   The interstitial region around and between the micelles is a solvent and corona (PEO) filled region.   This is a simple schematic and the details of the interstitial regions should be interpreted with caution; but one goal of this work is an improved understanding of this region.

<< Figure 10 >>

Physical obstructions impact diffusion in gels, with diffusivity decreasing proportionally to the volume fraction of obstruction. Here, the impact of PPO cores as obstructions in the ordered micellar system is considered. The reduced diffusivity can be expressed as $D/D_0 = (1-\alpha\phi)$ where α is a shape factor that is 3/2 for spheres, and ϕ is the volume fraction of obstructions.[55] For this system, the PPO micellar cores create the obstructions and their volume fraction is estimated by assuming fully dehydrated PPO cores and calculating the volume fraction of the cores for a given unit cell.[11]   Table 2 shows the values for R_{core} and ϕ_c, showing that the PPO core occupies a small fraction of the sample volume. The predicted reduction in diffusivity from the PPO obstructions is no more than 20%, which is not likely to be the cause of the drop in D observed in Figure 3. However, in the case of P123, the probe size approaches that of the distance between the PPO cores.

SANS measurements suggest that BSA and other similarly sized particles template within the interstitial regions of the ordered block copolymer micelles. Because the block copolymer-nanoparticle composite structure resembles that of an intercalated crystal, the probe particle diffusivity in the ordered micellar phases is modeled here with an interstitial diffusion mechanism similar to atom migration in solid crystalline materials.[56] In interstitial diffusion, the diffusion coefficient is related to the crystal dimension as $D = \Gamma r^2/6$, where Γ is the total jump rate of the particle, and r^2 is the jump distance. The jump distance can be written in terms of the lattice parameter a, which is dependent on the specific crystalline structure; for a BCC structure, $r_{bcc}=a/2$, while for an FCC crystal $r_{fcc}= 2^{1/2}a/2$. Thus, $D_{BCC} = \Gamma a^2/24$ and $D_{FCC}= \Gamma a^2/12$. For the block copolymers in this study, the lattice parameters of the ordered micellar structures are obtained through SANS measurements, and the lattice parameter scales inversely with polymer concentration in the concentration range studied, $a \sim 1/c$.[21, 23] Other experimental observations on these block copolymers also note an inverse relationship between the lattice parameter and polymer concentration.[57] Then,

$$D \sim \Gamma c^{-2}, \tag{5}$$

where c is polymer concentration. From the open symbols in Figure 4, this underestimates the dependence of D on concentration if Γ is not a function of concentration.   So, an attempt is made to provide an expression for the jump rate. The total jump rate of the particle in the material is $\Gamma = Zv\exp(-\Delta E/kT)$, where Z is the number of nearest interstitial sites ($Z_{BCC}=4$, $Z_{FCC}=12$), v is the attempt frequency of the particle, ΔE is the energy barrier that the particle must overcome in order to successfully move from one interstice to another, k is the Boltzmann constant, and T the temperature. The product $v\exp(-\Delta E/kT)$ is the jump rate of one particle from one site to a neighboring site and describes the frequency at which the particle is able to successfully complete the jump. Since the BSA is diffusing through the PEO coronas of the micelles, we treat the environment as one of a polymer solution so the energy barrier is regarded as the elastic energy of deformation that the polymer network experiences to accommodate passage of the probe particle through the micellar structures. In this case, $\Delta E \sim kT\gamma(d/\xi)^2$, where γ is related to the number of polymer meshes that undergo deformation, d is the probe particle diameter, and ξ is the characteristic size of the unperturbed polymer network. In a good solvent, ξ is related to polymer concentration, c, as $\xi \sim c^{-3/4}$.[45, 58, 59] So diffusion from an activated hopping process in these micellar crystals will have a complex dependence on concentration,

$$D(c) \sim \beta'c^{-2}\exp(-\gamma d^2 c^{3/2}) \tag{6}$$

where β' is a prefactor related to the crystal geometry and jump attempt frequency, and γ is a prefactor related to the number of polymer chains involved in the stretching of the network.

14

The open symbols in Figure 4 show the BSA diffusivity in soft solids with enough nanoscale structure to be studied with this simple model. While an exponential dependence of reduced diffusion coefficient on concentration is observed, there is not enough data to study the detailed $D(c)$ suggested by Equation (6) for samples in the ordered micellar phase. In all three cases, the value of D in the soft solid follows an exponential dependence on concentration.   With limited data, all that should be extracted is that the slope of this dependence is similar for F87 and F127, but higher for P123.   Since this slope, and γ, is proportional to the number of polymer chains that are deformed during the jumping process. Then, the overall energy required for jumping to occur will increase for a system with more densely packed coronas. Of the three systems, P123 has the highest aggregation number, followed by F87 and then F127,[7, 9] which is consistent with the physical description suggested by the model. While both F127 and P123 form FCC configurations in the ordered micellar phases, the PEO block length is nearly four times shorter in P123 than in F127. As a result, the P123 corona size, which ranges from approximately 1-2 nm, is very nearly the same as the BSA radius ($R_o \sim 3.5$nm) which would be more restrictive to BSA diffusivity than the F127 corona size of ~2-3nm.

Conclusions

The complexity that self-assembling block copolymers exhibit in their structural and mechanical properties clearly extends to nanoparticle transport through these systems, with results indicating that nanoparticle diffusivity is sensitive to block copolymer type, concentration, and structure. The resulting range of protein diffusivity spans across many orders of magnitude for the concentrations studied, and demonstrates the versatility of these self-assembled systems for controlling nanoparticle transport. Macroscopic properties are not enough to predict the level of hindrance to transport observed, the architecture of the block copolymer and micelle structure need to be considered. In a solution of concentrated micelles (near C_{gl}, defined mechanically), probes of similar size to the micelles exhibit scaling expected for diffusion through a polymer solution with probe size similar to the correlation length of the polymer solution.   The transition of the block copolymer micelle solution to a soft solid does not result in a discontinuous drop in probe diffusivity. In the soft solid the more relevant length scale will be those of the unit cell.

Acknowledgements

References

1. F. S. Bates and G. H. Fredrickson, *Annu Rev Phys Chem*, 1990, 41, 525-557.
2. I. W. Hamley, *Journal of Physics-Condensed Matter*, 2001, 13, R643-R671.
3. T. P. Lodge, *Macromolecular Chemistry and Physics*, 2003, 204, 265-273.
4. K. Mortensen, W. Brown and B. Norden, *Physical Review Letters*, 1992, 68, 2340-2343.
5. P. Alexandridis, J. F. Holzwarth and T. A. Hatton, *Macromolecules*, 1994, 27, 2414-2425.
6. P. Alexandridis and T. A. Hatton, *Colloids and Surfaces a-Physicochemical and Engineering Aspects*, 1995, 96, 1-46.
7. G. Wanka, H. Hoffmann and W. Ulbricht, *Macromolecules*, 1994, 27, 4145-4159.
8. K. Mortensen, *J. Phys.: Condensed Matter*, 1996, 8, A103-A124.
9. K. Mortensen and W. Brown, *Macromolecules*, 1993, 26, 4128-4135.
10. P. Linse, *Macromolecules*, 1993, 26, 4437-4449.
11. R. K. Prudhomme, G. W. Wu and D. K. Schneider, *Langmuir*, 1996, 12, 4651-4659.
12. I. Goldmints, G. E. Yu, C. Booth, K. A. Smith and T. A. Hatton, *Langmuir*, 1999, 15, 1651-1656.
13. I. W. Hamley and V. Castelletto, *Prog Polym Sci*, 2004, 29, 909-948.
14. H. Yardimci, B. Chung, J. L. Harden and R. L. Leheny, *Journal of Chemical Physics*, 2005, 123.
15. D. C. Pozzo, K. R. Hollabaugh and L. M. Walker, *Journal of Rheology*, 2005, 49, 759-782.
16. D. C. Pozzo and L. M. Walker, *Macromolecular Symposia*, 2005, 227, 203-210.
17. D. C. Pozzo and L. M. Walker, *Macromolecules*, 2007, 40, 5801-5811.
18. D. C. Pozzo and L. M. Walker, *Colloids and Surfaces a-Physicochemical and Engineering Aspects*, 2007, 294, 117-129.
19. D. C. Pozzo and L. M. Walker, *European Physical Journal E*, 2008, 26, 183-189.
20. A. Louhichi, E. Tamborini, J. Oberdisse, L. Cipelletti and L. Ramos, *Physical Review E*, 2015, 92.
21. T. A. LaFollette, Thesis (PhD), Carnegie Mellon University, 2010.
22. T. A. LaFollette and L. M. Walker, *Polymers*, 2011, 3, 281-298.
23. D. C. Pozzo, Thesis (PhD), Carnegie Mellon University, 2006.
24. M. R. Bockstaller, R. A. Mickiewicz and E. L. Thomas, *Advanced Materials*, 2005, 17, 1331-1349.
25. B. Sarkar and P. Alexandridis, *Prog Polym Sci*, 2015, 40, 33-62.
26. M. M. Domach and L. M. Walker, *JALA*, 2010, 15, 136-144.
27. A. W. Kirkeminde, T. Torres, T. Ito and D. A. Higgins, *Journal of Physical Chemistry B*, 2011, 115, 12736-12743.
28. R. Svingen, P. Alexandridis and B. Akerman, *Langmuir*, 2002, 18, 8616-8619.
29. L.-H. Cai, S. Panyukov and M. Rubinstein, *Macromolecules*, 2011, 44, 7853-7863.
30. Y. Cheng, R. K. Prud'homme and J. L. Thomas, *Macromolecules*, 2002, 35, 8111-8121.
31. G. D. J. Phillies, G. S. Ullmann, K. Ullmann and T. H. Lin, *Journal of Chemical Physics*, 1985, 82, 5242-5246.
32. J. Won, C. Onyenemezu, W. G. Miller and T. P. Lodge, *Macromolecules*, 1994, 27, 7389-7396.
33. I. Kohli and A. Mukhopadhyay, *Macromolecules*, 2012, 45, 6143-6149.

34. R. Holyst, A. Bielejewska, J. Szymanski, A. Wilk, A. Patkowski, J. Gapinski, A. Zywocinski, T. Kalwarczyk, E. Kalwarczyk, M. Tabaka, N. Ziebacz and S. A. Wieczorek, *Physical Chemistry Chemical Physics*, 2009, 11, 9025-9032.
35. T. K. L. Meyvis, S. C. De Smedt, P. Van Oostveldt and J. Demeester, *Pharmaceutical Research*, 1999, 16, 1153-1162.
36. E. M. Johnson, D. A. Berk, R. K. Jain and W. M. Deen, *Biophys J*, 1996, 70, 1017-1023.
37. E. E. Holly, S. K. Venkataraman, F. Chambon and H. H. Winter, *Journal of Non-Newtonian Fluid Mechanics*, 1988, 27, 17-26.
38. T. H. The and T. E. Feltkamp, *Immunology*, 1970, 18, 865-&.
39. T. H. The and T. E. Feltkamp, *Immunology*, 1970, 18, 875-&.
40. Pierce Biotechnology: FITC and TRITC, http://www.piercenet.com/instructions/2162081.pdf).
41. M. Malmsten, *Biopolymers at interfaces / edited by Martin Malmsten*, Marcel Dekker, New York, 2nd edn., 2003.
42. R. D. Phair, S. A. Gorski and T. Misteli, *Method Enzymol*, 2004, 375, 393-414.
43. J. Tong and J. L. Anderson, *Biophys J*, 1996, 70, 1505-1513.
44. S. Gupta, J. Stellbrink, E. Zaccarelli, C. N. Likos, M. Camargo, P. Holmqvist, J. Allgaier, L. Willner and D. Richter, *Physical Review Letters*, 2015, 115.
45. M. Rubinstein and R. H. Colby, *Polymer physics*, Oxford University Press, Oxford ; New York, 2003.
46. L. C. P. Trong, M. Djabourov and A. Ponton, *Journal of Colloid and Interface Science*, 2008, 328, 278-287.
47. V. Castelletto, I. W. Hamley and T. A. Waigh, *J. Chemical Physics*, 2004, 121, 111474.
48. L. R. G. Treloar, *The physics of rubber elasticity* Clarendon Press ;Oxford University Press, Oxford, New York, 3rd edn., 2005.
49. C. T. Reinhart and N. A. Peppas, *J Membrane Sci*, 1984, 18, 227-239.
50. M. S. Green and A. V. Tobolsky, *Journal of Chemical Physics*, 1946, 14, 80-92.
51. K. Devanand and J. C. Selser, *Macromolecules*, 1991, 24, 5943-5947.
52. L.-H. Cai, S. Panyukov and M. Rubinstein, *Macromolecules*, 2015, 48, 847-862.
53. K. Devanand and J. C. Selser, *Nature*, 1990, 343, 739-741.
54. S. Kawaguchi, G. Imai, J. Suzuki, A. Miyahara and T. Kitano, *Polymer*, 1997, 38, 2885-2891.
55. M. A. Lauffer, *Biophys J*, 1961, 1, 205-&.
56. R. W. Balluffi, S. M. Allen, W. C. Carter and R. A. Kemper, *Kinetics of materials*, J. Wiley & Sons, Hoboken, N.J., 2005.
57. P. Alexandridis, D. L. Zhou and A. Khan, *Langmuir*, 1996, 12, 2690-2700.
58. A. Halperin, M. Tirrell and T. P. Lodge, in *Macromolecules: Synthesis, Order and Advanced Properties*, Springer Berlin Heidelberg, 1992, vol. 100/1, ch. 3, pp. 31-71.
59. P. G. Degennes, *Journal of Chemical Physics*, 1982, 76, 3316-3321.
60. B. Lindman and P. Alexandridis, *Amphiphilic block copolymers : self-assembly and applications*, Elsevier, Amsterdam ; New YOrk, 1st edn., 2000.
61. J. R. Lopes and W. Loh, *Langmuir*, 1998, 14, 750-756.
62. R. Bhat and S. N. Timasheff, *Protein Sci*, 1992, 1, 1133-1143.

.

Table 1. Physical properties of different block copolymers, with molecular formula PEO_x-PPO_y-PEO_x. Molecular properties are reported by the manufacturer, the critical micelle concentration (CMC) at 25^oC is reported in the literature. The transition concentration, C_{gl}, is determined here.

Polymer	Molecular Weight (g/mol)	PEO units (x)	PPO units (y)	PEO:PPO Ratio	CMC [60, 61]	C_{gl} (wt%)
P123	5750	20	70	0.57	0.03	28
F127	12600	106	70	3.0	1	18
F87	7700	75	46	3.3	2	34

Table 2. Corresponding micellar core dimensions and volume fraction for different block copolymer compositions obtained from SANS measurements and literature (T=25°C).

Polymer	Conc. (wt%)	Crystal Lattice	Unit cell lattice (nm)	Hard sphere radius (nm)	R_{core} (nm)	ϕ_{core}	R_g PEO[62] (nm)
F127	25	FCC	28.7	10.2	3.8	0.04	2.7
F87	40	BCC	15.6	6.8	3.7	0.11	2.3
P123	35	FCC	25.3	9.0	5.1	0.13	1.3
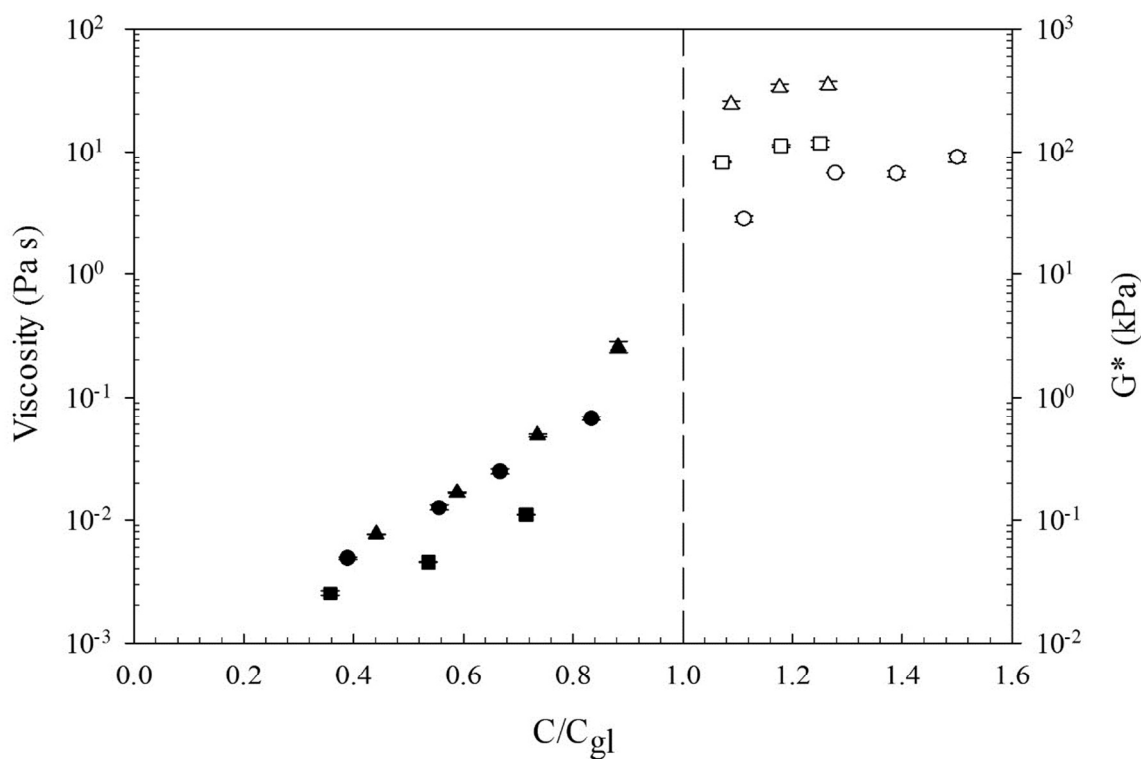
Figure 1. Zero shear rate viscosity and complex modulus (small amplitude, 1 rad/s) for block copolymer samples in the fluid (filled symbols) and micellar crystal (open symbols) phases, measured at T=25°C. Block copolymer concentration has been normalized by C_{gl}. The symbols correspond to F127 (●), F87 (▲), and P123 (■).
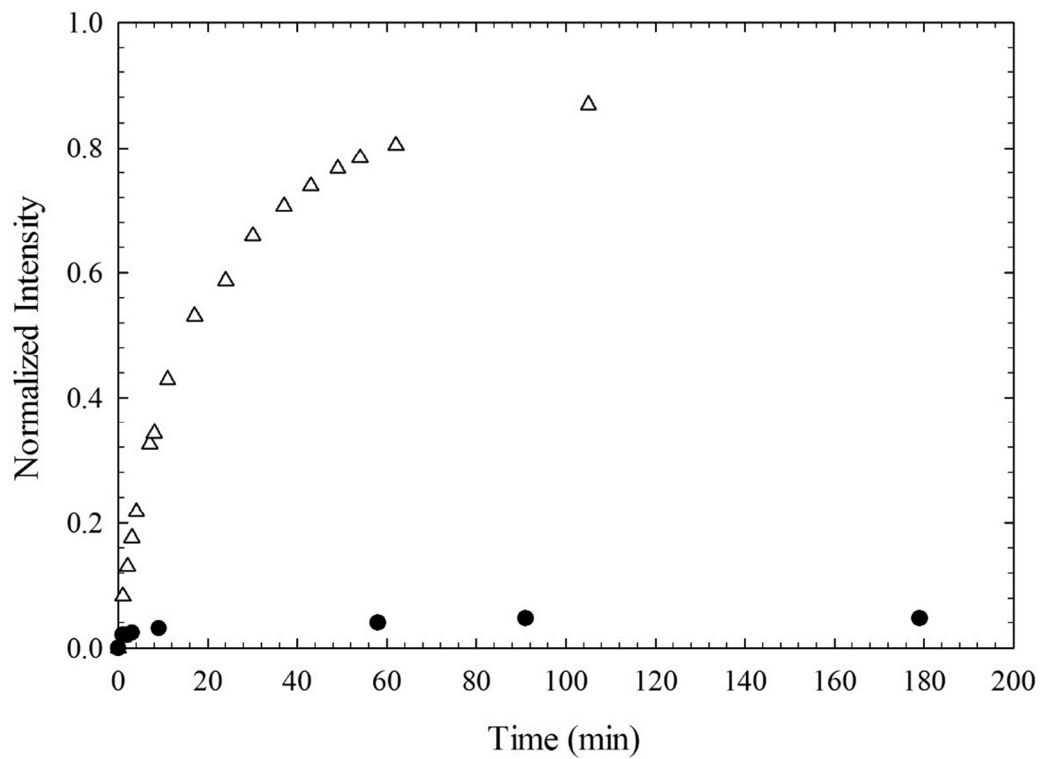
Figure 2. Fluorescence intensity normalized to the value immediately after photobleaching, as a function of time for FITC-BSA (open symbols) and hydrophobic HDFL dye (filled symbols) in 25 wt% F127 (C/C_{gl} = 1.4) at ambient temperature.

20
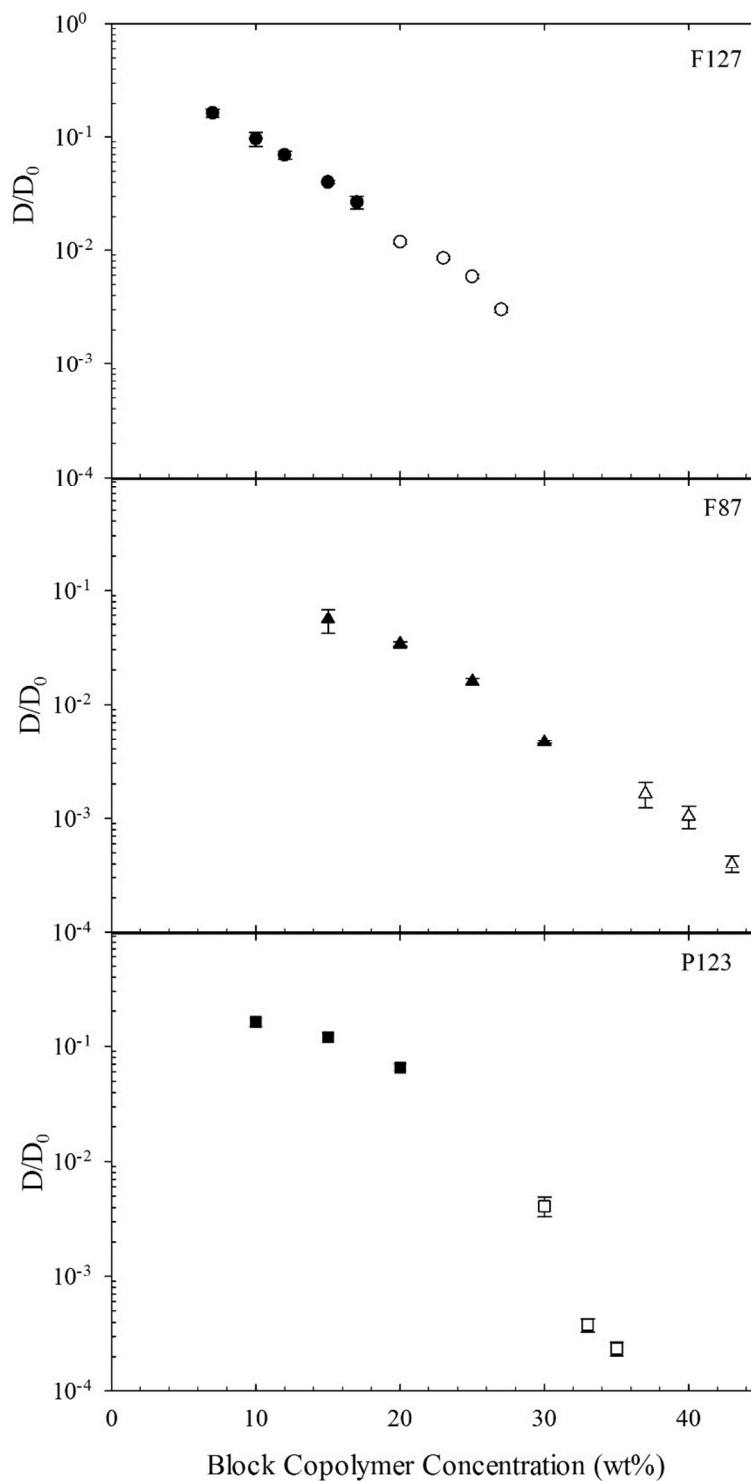
Figure 3. The normalized FITC-BSA diffusivity (D_o is the diffusivity of BSA in water) as a function of block copolymer concentration for both disordered fluid (filled symbols, $C < C_{gl}$) and ordered micelle (open symbols, $C > C_{gl}$) concentrations and ambient temperature.
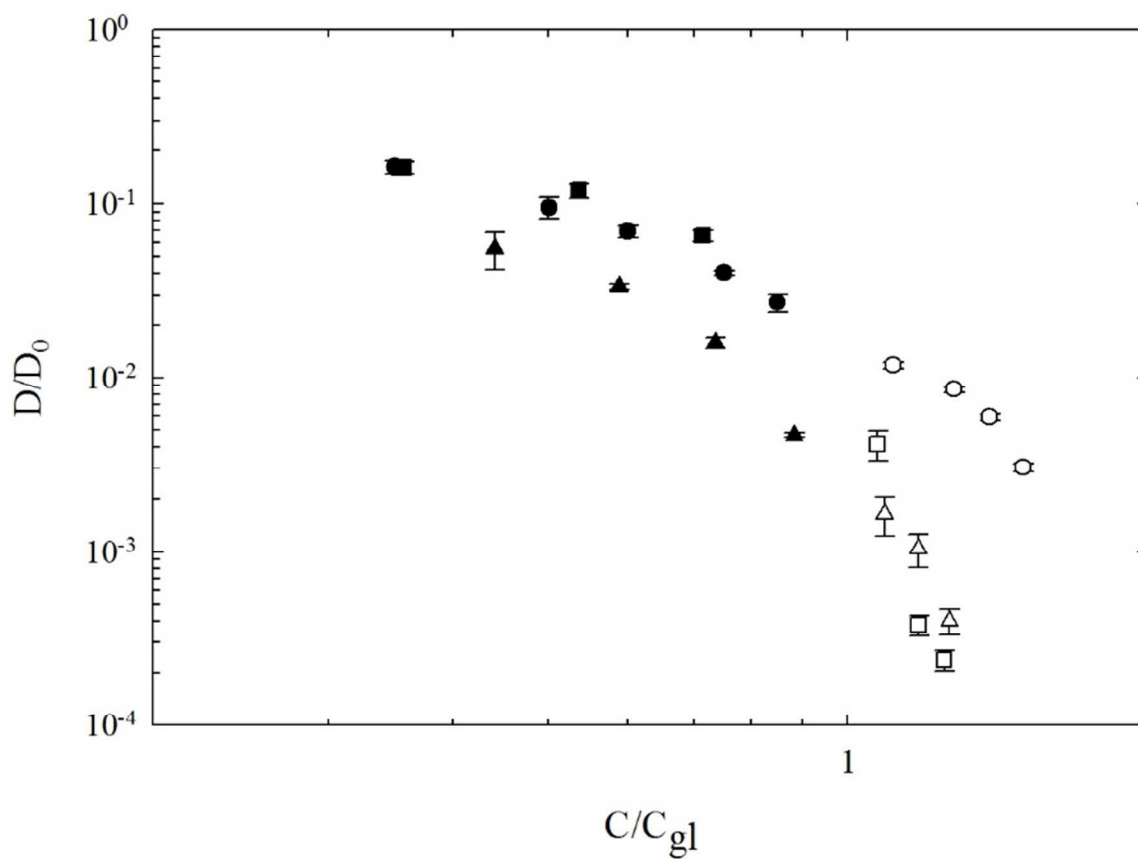
Figure 4: The normalized FITC-BSA diffusivity (D_o is the diffusivity of BSA in water) as a function of block copolymer concentration for both disordered fluid (filled symbols, $C < C_{gl}$) and ordered micelle (open symbols, $C > C_{gl}$) concentrations and ambient temperature.
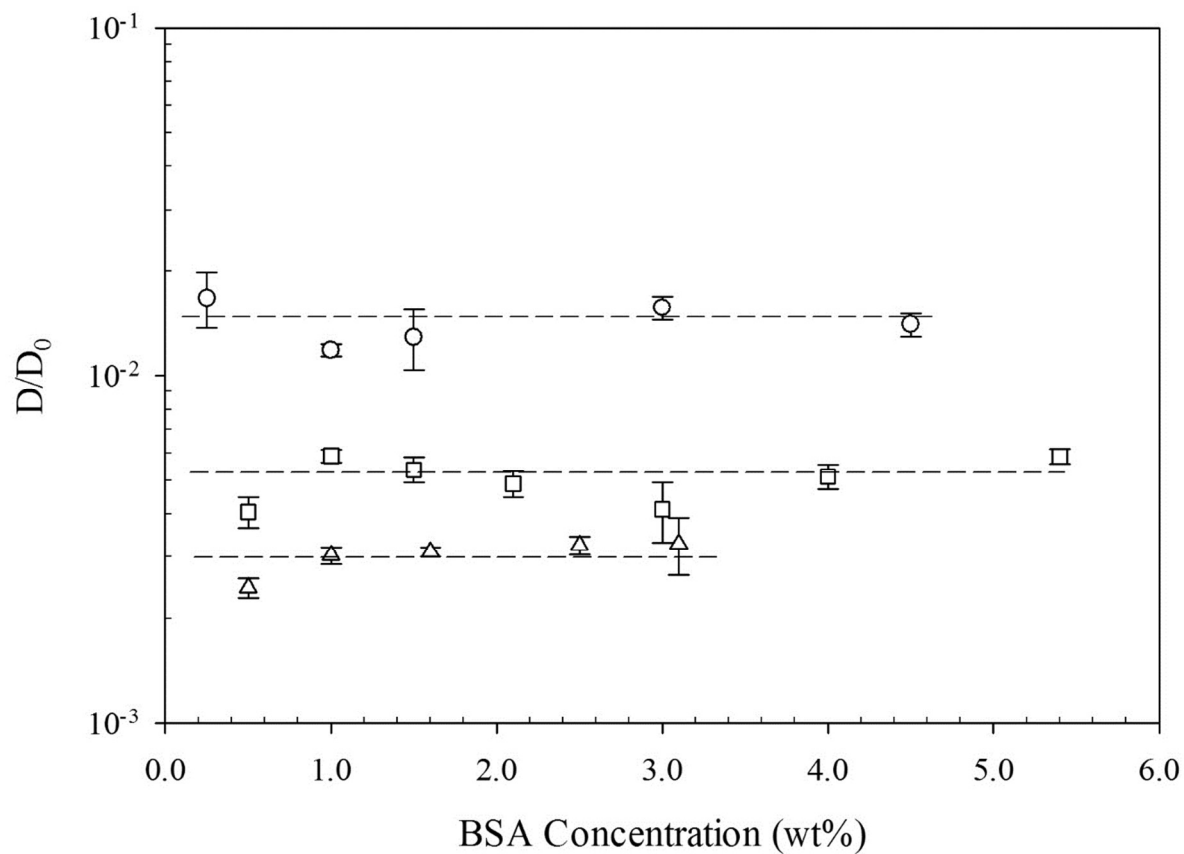
Figure 5. Reduced diffusivity as a function of total BSA particle loading. Three different block copolymer concentrations are examined: 20 wt% F127 (○), 25 wt% F127 (□) and 27 wt% F127 (△).
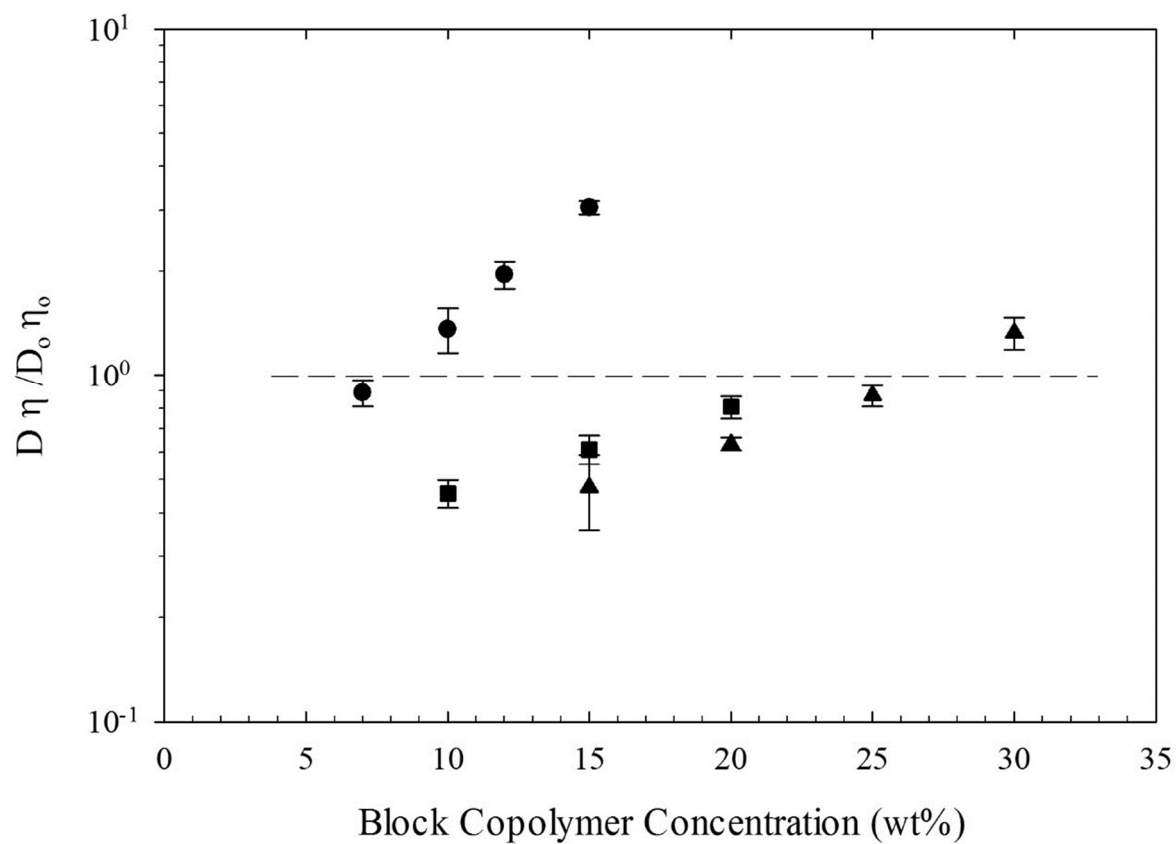
Figure 6. $D\eta/D_o\eta_o$, normalized relative to free solution values for FITC-BSA in block copolymer solutions F127 (●), F87 (▲), and P123 (■) at concentrations below C_{gl}. The dashed line shows the expected behavior for a probe undergoing Stokes-Einstein-Sutherland diffusion.
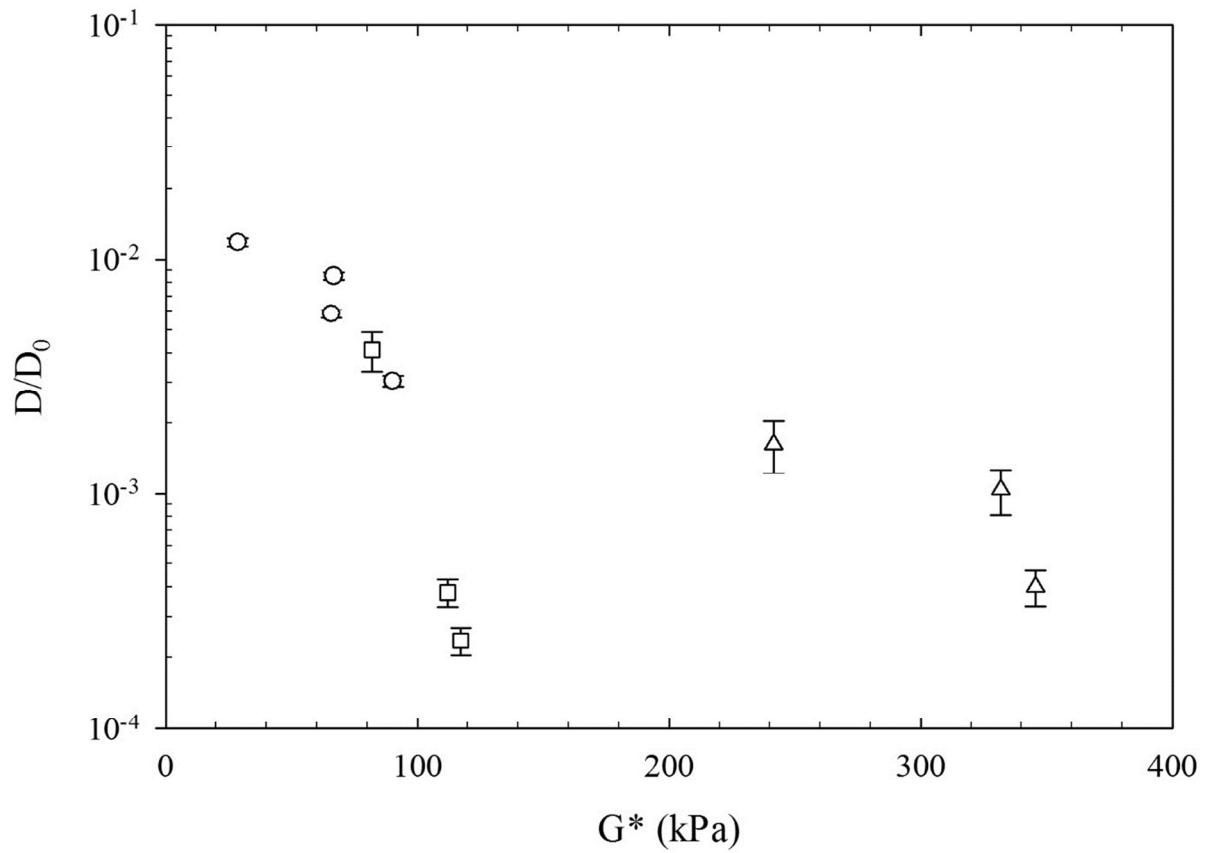
Figure 7. Reduced diffusivity of FITC-BSA as a function of complex modulus of the composite for the block copolymer solutions at $C > C_{gl}$ and room temperature. Symbols correspond to F127 ($\bigcirc$), F87 ($\triangle$) and P123 ($\square$).
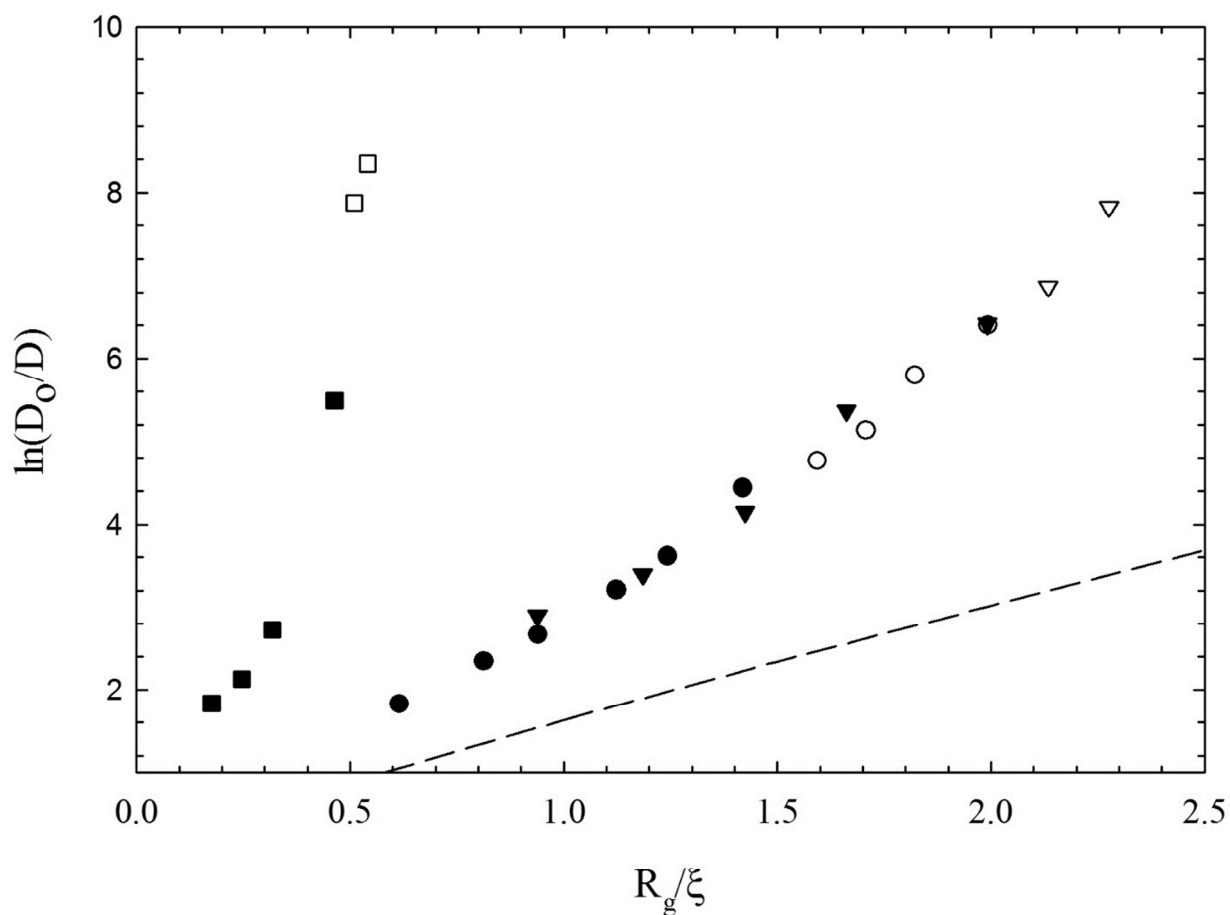
Figure 8: Inverse of the reduced diffusivity of FITC-BSA as a function of polymer radius of gyration over correlation length for each of the block copolymer systems below (filled) and above (open) the C_{gl}. Symbol shapes are the same as the previous figures. The dashed line represents the measured relationship presented by Kohli *et al.* [33] for gold nanoparticles diffusing through PEO solutions.
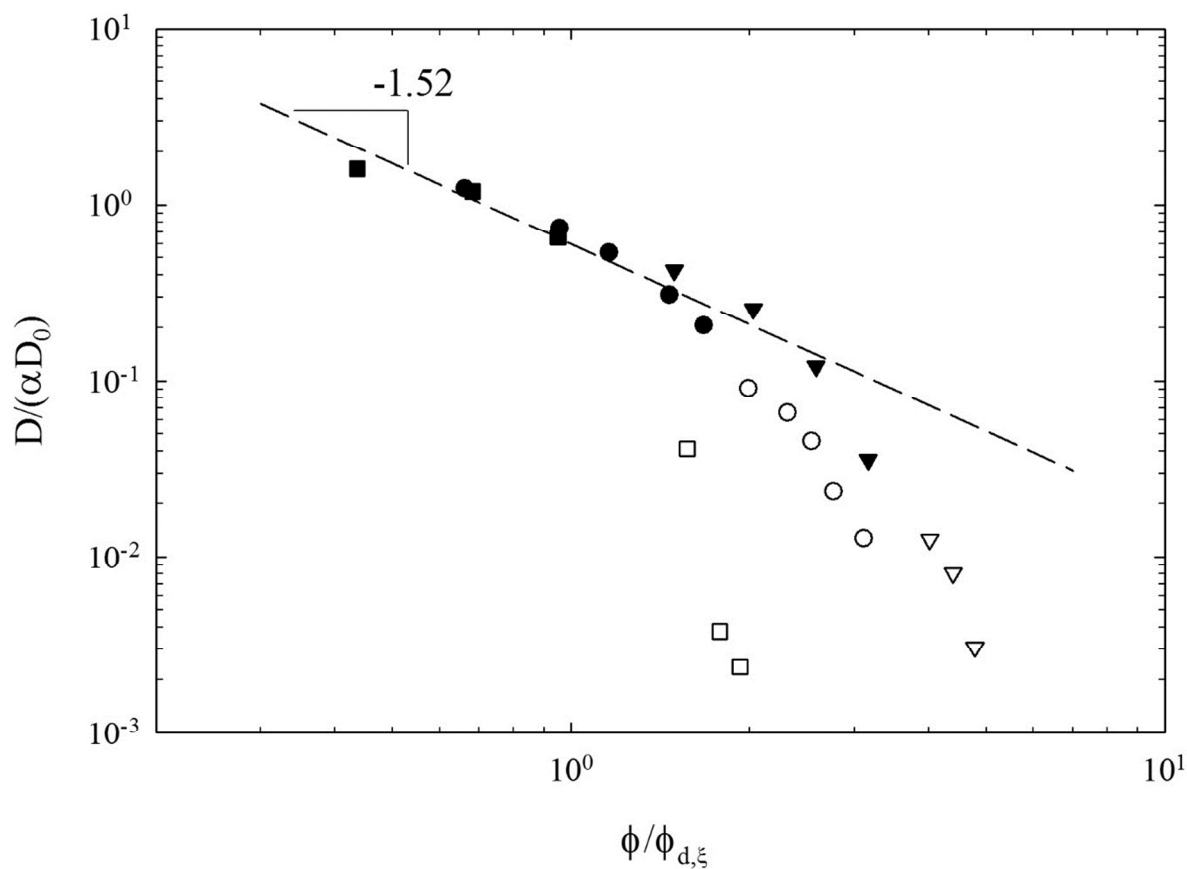
Figure 9. Reduced diffusivity of FITC-BSA as a function of normalized polymer concentration for each of the block copolymer systems below (filled) and above (open) the C_{gl}. Symbol shapes are the same as the previous figures. The dashed line represents the scaling relationship presented by Cai *et al.*[29] for non-sticky nanoparticles diffusing through polymer solutions.
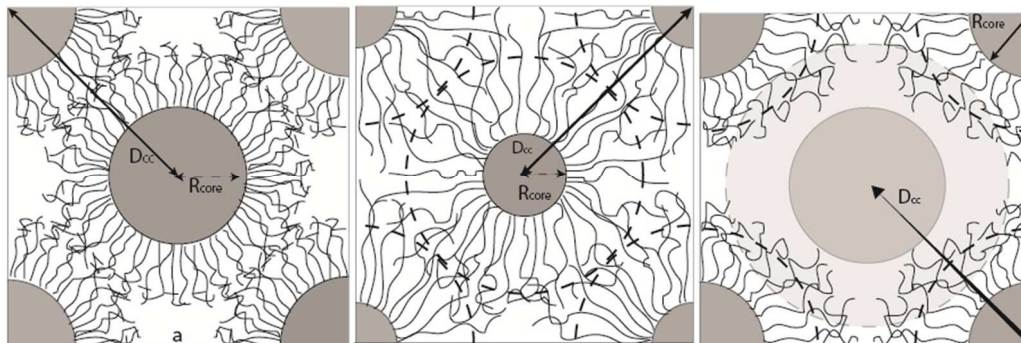
Figure 10. Unit cell depictions of P123 (left), F127 (center), and F87 (right), with micelle cores depicted as dark grey regions. Unit cell size and structure are determined from small angle scattering. The PPO core is estimated by assuming a fully dehydrated core. The dotted line is micelle size determined by assuming hard spheres packed in a crystal. P123 and F127 form FCC crystals, while F87 forms a BCC crystal. Dimensions are provided in Table 2.